nature astronomy

SUPPLEMENTARY INFORMATION

DOI: 10.1038/s41550-017-0264-4

In the format provided by the authors and unedited.

Tidally disrupted dusty clumps as the origin of broad emission lines in active galactic nuclei

Jian-Min Wang[1,2,3]*, Pu Du[1], Michael S. Brotherton[4], Chen Hu[1], Yu-Yang Songsheng[1], Yan-Rong Li[1], Yong Shi[5] and Zhi-Xiang Zhang[1]

[1]Key Laboratory for Particle Astrophysics, Institute of High Energy Physics, Chinese Academy of Sciences, 19B Yuquan Road, 100049 Beijing, China. [2]School of Astronomy and Space Sciences, and School of Physical Sciences, University of Chinese Academy of Sciences, 19A Yuquan Road, 100049 Beijing, China. [3]National Astronomical Observatories of China, Chinese Academy of Sciences, 20A Datun Road, 100020 Beijing, China. [4]Department of Physics and Astronomy, University of Wyoming, Laramie, WY 82071, USA. [5]School of Astronomy and Space Science, Nanjing University, 210093 Nanjing, China. *e-mail: wangjm@ihep.ac.cn

The broad-line region of active galactic nuclei: tidally disrupted clumps from the torus

Jian-Min Wang, Pu Du, Michael S. Brotherton, Chen Hu, Yu-Yang Songsheng, Yan-Rong Li, Yong Shi and Zhi-Xiang Zhang

Supplementary Table 1

A list of parameters involved in the present model

Parameter	Physical meanings	Valid ranges	Uncertainties ($\langle \Delta X/X \rangle$)
ζ_0	$R_{\rm T}^0 \omega_{\rm A}^0 / v_{\rm A}^0$: determines trajectories of clumps	$0 \sim 50$	1.6
$\gamma_{\rm A}$	cloud A distribution index: $N_{\rm A} = N_{\rm A}^0 v_{\rm A}^{\gamma_{\rm A}}$	$0 - 4$	0.5
$\xi_{\rm A}$	$v_{\rm A}^0 = \xi_{\rm A} \left(\zeta_0^2 + 1\right)^{-1/2} v_{\rm K}^0$, $v_{\rm K}^0$ is the Keplerian velocity at $R_{\rm T}^0$.	< 1	0.2
$R_0/R_{\rm g}$	the circulaized radius of type A clouds	$\sim 6.2 \times 10^3$	0.3
$R_{\rm in}$	radius of type B clouds merging with accretion disks	$< R_{\rm BLR}$	0.6
$\gamma_{\rm B}$	cloud B distribution index: $N_{\rm B} = N_{\rm B}^0 v_{\rm B}^{\gamma_{\rm B}}$	$0 - 4$	0.5
$f_{\rm B}$	fraction of type B clouds	$0 \sim 1$	0.3
$\xi_{\rm C}$	$v_{\rm C}^0 = \xi_{\rm C} v_{\rm K}^0$, $v_{\rm C}^0$ is the ejection velocity of type C clouds at $R_{\rm T}^0$.	> 1	0.3
$f_{\rm C}$	fraction of type C clouds, properties shown by Equation (7)	$0 \sim 1$	0.6
i	inclination angle of observers, $i = 0^\circ$ (edge-on) and $i = 90^\circ$(face-on)	$\gtrsim 40^\circ$	0.2
	Auxiliary Parameters (the fixed values are listed by the numbers in bold fonts)		
$\Theta_{\rm torus}$	half angle of torus given by the $\Theta_{\rm torus} - L_{\rm [OIII]}$ relation	Ref.[1]	
$\alpha_{\rm A}$	cloud A velocity index: $v_{\rm A} = v_{\rm A}^0 \left(R/R_{\rm T}^0\right)^{-\alpha_{\rm A}}$	$\mathbf{0.45}$; ≤ 0.5	
$\alpha_{\rm C}$	cloud C velocity index: $v_{\rm C} = v_{\rm C}^0 \left(R/R_{\rm T}^0\right)^{-\alpha_{\rm C}}$	$\mathbf{0.30}$; ≤ 0.5	
$\beta_{\rm A}$	cloud A angular velocity index: $\omega_{\rm A} = \omega_{\rm A}^0 \left(R/R_{\rm T}^0\right)^{-\beta_{\rm A}}$	$\mathbf{1.8}$; ≥ 1.5	
$\gamma_{\rm C}$	cloud C distribution index: $N_{\rm C} = N_{\rm C}^0 v_{\rm C}^{\gamma_{\rm C}}$	$\mathbf{0}$; ~ 0.5	
γ	vertical distribution of clumps in torus: $\propto (\cos\theta_{\rm C})^{\gamma}$	$\mathbf{1}$; ~ 1	
Γ	$1 + \alpha_{\rm A} - \beta_{\rm A}$		
$R_{\rm T}^0/R_{\rm g}$	tidal disruption radius of clumps.	$\mathbf{10^4}$; $(R_0, R_{\rm torus})$	
$R_{\rm BLR}$	the emissivity-averaged radius of the BLR determined by RM.		
φ_0	position angle of tidal event.	$\varphi_0 = \pi/2$	
$\omega_{\rm A}^0$	angular velocity of type A clouds at $R_{\rm T}^0$.	absorbed by ζ_0	

Note: the averaged $\langle \Delta X/X \rangle$ is obtained by the statistic of individual $\Delta X/X$ of the sample. Here X is any one of the fitting parameters in the model.

Supplementary Table 2

Resultant parameters of best-fittings of four quasars

Parameter	PG1354+213	PG2251+113	PG1351+640	PG1700+518
ζ_0	6.1^{+10}_{-6}	$0.71^{+1.5}_{-0.5}$	$0.02^{+5}_{-0.02}$	38^{+13}_{-31}
$\xi_{\rm A}$	$0.36^{+0.3}_{-0.1}$	$0.59^{+0.2}_{-0.1}$	$0.42^{+0.1}_{-0.1}$	$0.63^{+0.1}_{-0.1}$
$\gamma_{\rm A}$	$0.79^{+1.4}_{-0.79}$	$3.6^{+0.9}_{-1.8}$	$0.51^{+0.9}_{-0.2}$	$1.5^{+0.9}_{-0.5}$
$R_0(10^3R_{\rm g})$	$3.2^{+1.2}_{-0.9}$	$2.6^{+1.0}_{-0.7}$	$1.4^{+1.5}_{-0.8}$	$7.5^{+1.5}_{-2.5}$
$R_{\rm in}(10^3R_{\rm g})$	$0.31^{+0.2}_{-0.1}$	$0.38^{+0.1}_{-0.1}$	$0.39^{+0.1}_{-0.1}$	$3.6^{+1.3}_{-0.9}$
$\gamma_{\rm B}$	$1.2^{+0.1}_{-0.1}$	$2.1^{+0.9}_{-1.0}$	$2.8^{+0.9}_{-1.8}$	$3.0^{+0.9}_{-1.3}$
$f_{\rm B}$	$0.95^{+0.1}_{-0.6}$	$0.78^{+0.1}_{-0.2}$	$0.73^{+0.1}_{-0.1}$	$0.24^{+0.0}_{-0.1}$
$\xi_{\rm C}$	$2.7^{+0.5}_{-1.1}$	$1.1^{+0.2}_{-0.5}$	$2.2^{+0.1}_{-0.4}$	$2.9^{+0.1}_{-0.1}$
$f_{\rm C}$	$0.02^{+0.1}_{-0.02}$	$0.18^{+0.1}_{-0.1}$	$0.04^{+0.01}_{-0.01}$	$0.44^{+0.1}_{-0.1}$
$i(^\circ)$	75^{+8}_{-13}	66^{+9}_{-9}	74^{+5}_{-9}	61^{+2}_{-1}
		Line profiles		
$\mathcal{A}_{\rm H\beta}$	4.85	0.15	12.8	2.90
$\mathcal{S}_{\rm H\beta}$	0.30	0.22	1.41	1.07
$\mathcal{Z}_{\rm H\beta}$	1.34	1.12	1.77	2.15

Parameters of all the PG quasars will be provided on request.

Supplementary Table 3

Classifications of resultant fittings

Model	Number	Objects (total of 87 PG quasars)
B	1	1354+213
B+C	1	2251+113
A+B	12	0003+199, 0934+013, 1004+130, 1012+008, 1103-006, 1211+143, 1351+236
		1351+640, 1512+370, 1534+580, 1617+175, 2233+134
A+B+C	73	0003+158, 0007+106, 0026+129, 0043+039, 0049+171, 0050+124, 0052+251
		0157+001, 0804+761, 0838+770, 0844+349, 0921+525, 0923+129, 0923+201
		0947+396, 0953+414, 1001+054, 1011-040, 1022+519, 1048-090, 1048+342
		1049-006, 1100+772, 1114+445, 1115+407, 1116+215, 1119+120, 1121+422
		1126-041, 1149-110, 1151+117, 1202+281, 1216+069, 1226+023, 1229+204
		1244+026, 1259+593, 1302-102, 1307+085, 1309+355, 1310-108, 1322+659
		1341+258, 1352+183, 1402+261, 1404+226, 1411+442, 1415+451, 1416-129
		1425+267, 1426+015, 1427+480, 1435-067, 1440+356, 1444+407, 1448+273
		1501+106, 1519+226, 1535+547, 1543+489, 1545+210, 1552+085, 1612+261
		1613+658, 1626+554, 1700+518, 1704+608, 2112+059, 2130+099, 2209+184
		2214+139, 2304+042, 2308+098

B: $f_{\rm A,C} \leq 5\%$; B+C: $f_{\rm A} \leq 5\%$; A+B: $f_{\rm C} \leq 5\%$; A+B+C: $f_{\rm A,B,C} > 5\%$.

If it is less than 5%, we consider that component to be negligible. There are only two profiles with B and (B+C) components, only 12 objects with (A+B), while the majority of 73 objects employ (A+B+C). Generally, type B clouds are necessary in all objects, type A appears in 85/87 objects, and the type C in 74/87.

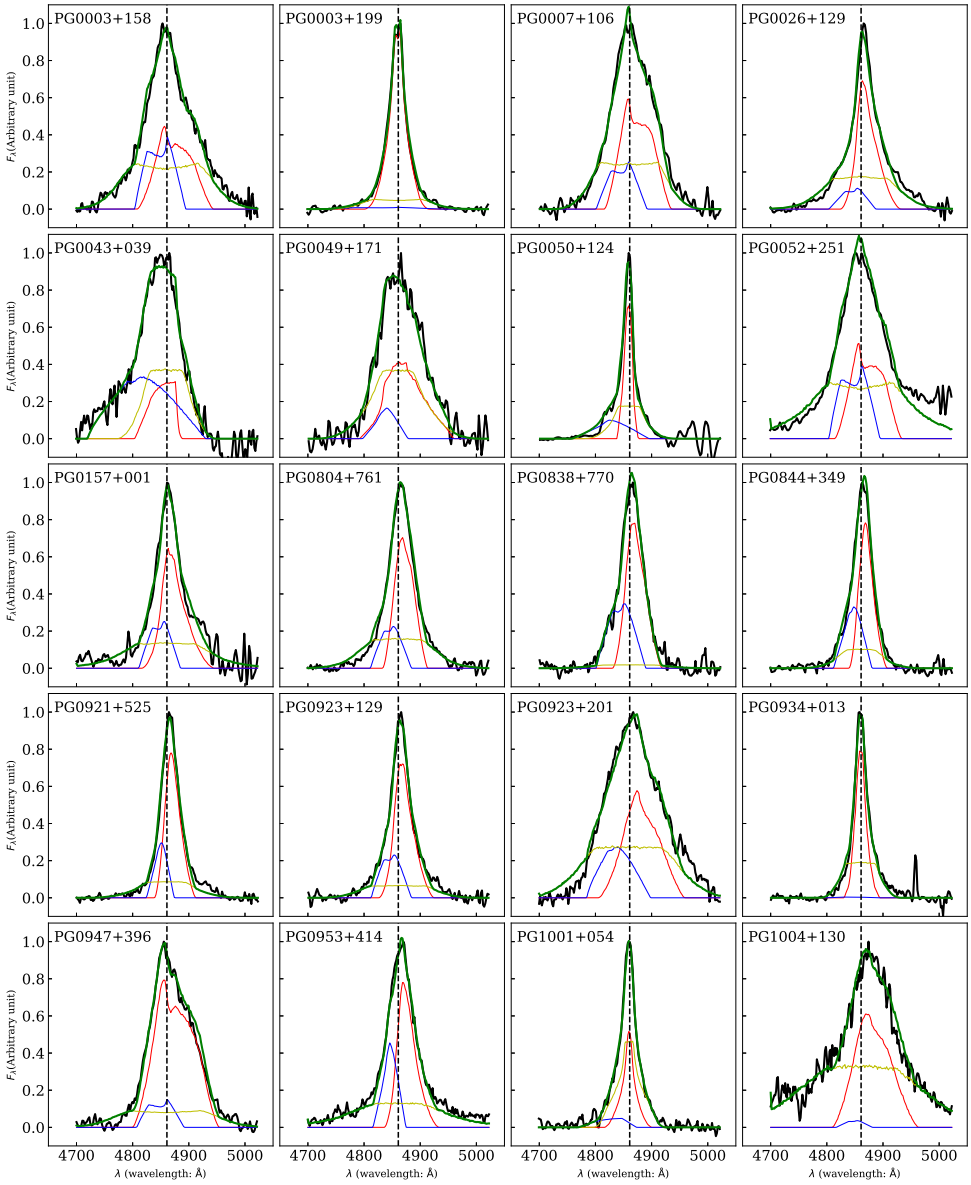

Supplementary Figure 1: **Comparisons of our model fits with observed Hβ profiles of PG quasars.** Solid black lines are the observed profiles, red lines are from type A clouds, the yellow from type B and the blue from type C and the green is the total of the three cloud types. The dashed lines are $\lambda_0 = 4861$Å.

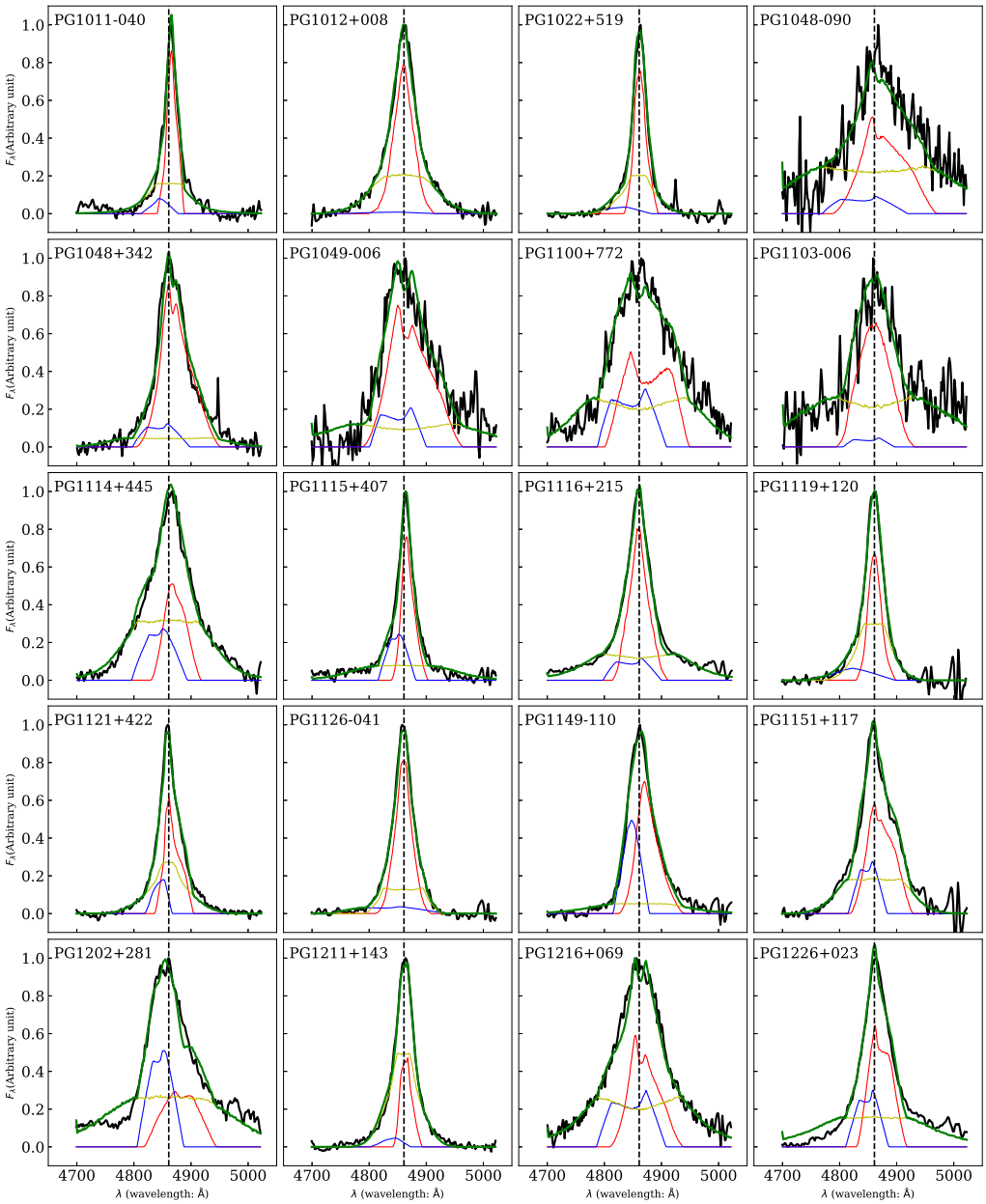

Supplementary Figure 1 *Continued*.

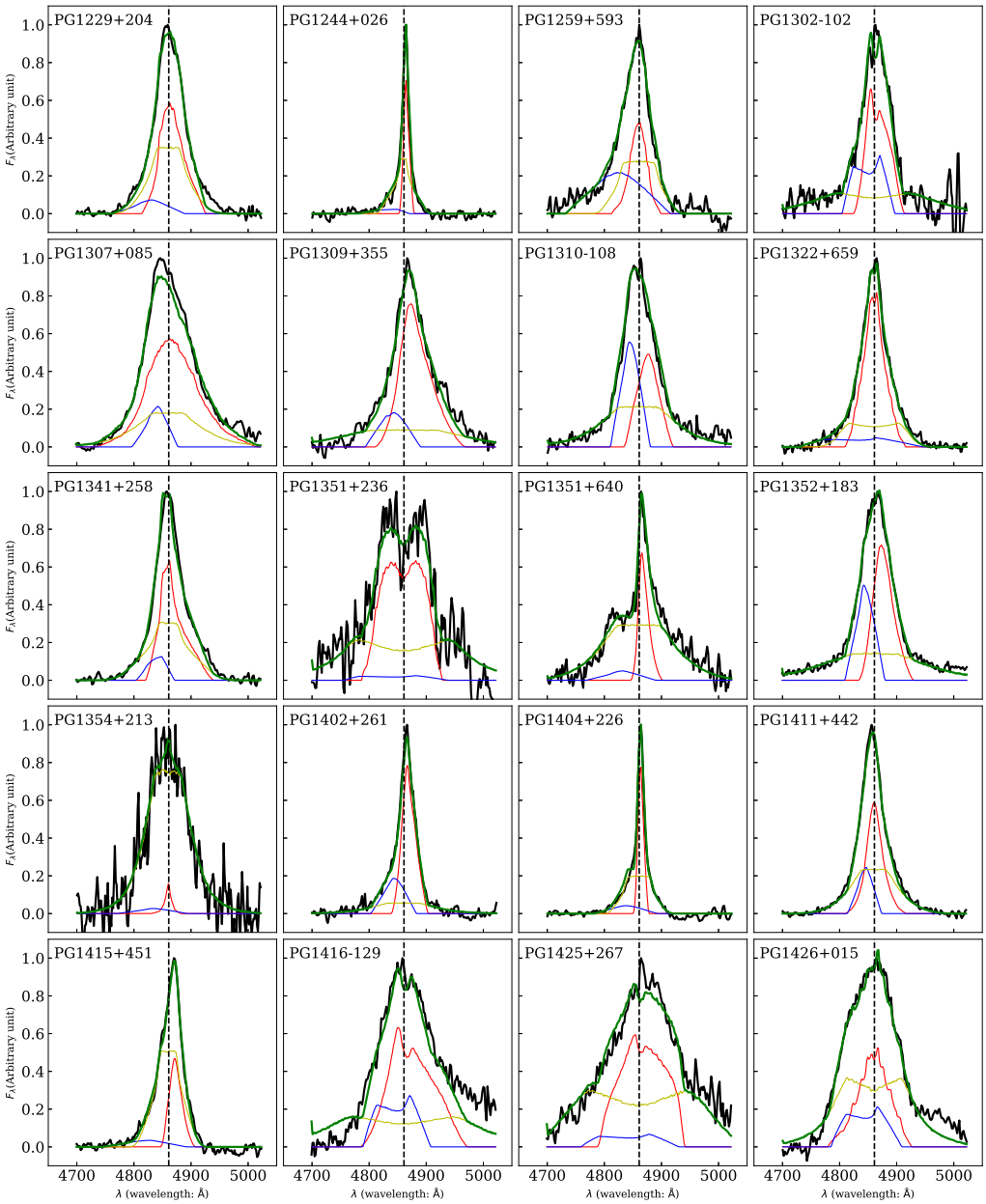

Supplementary Figure 1 *Continued*.

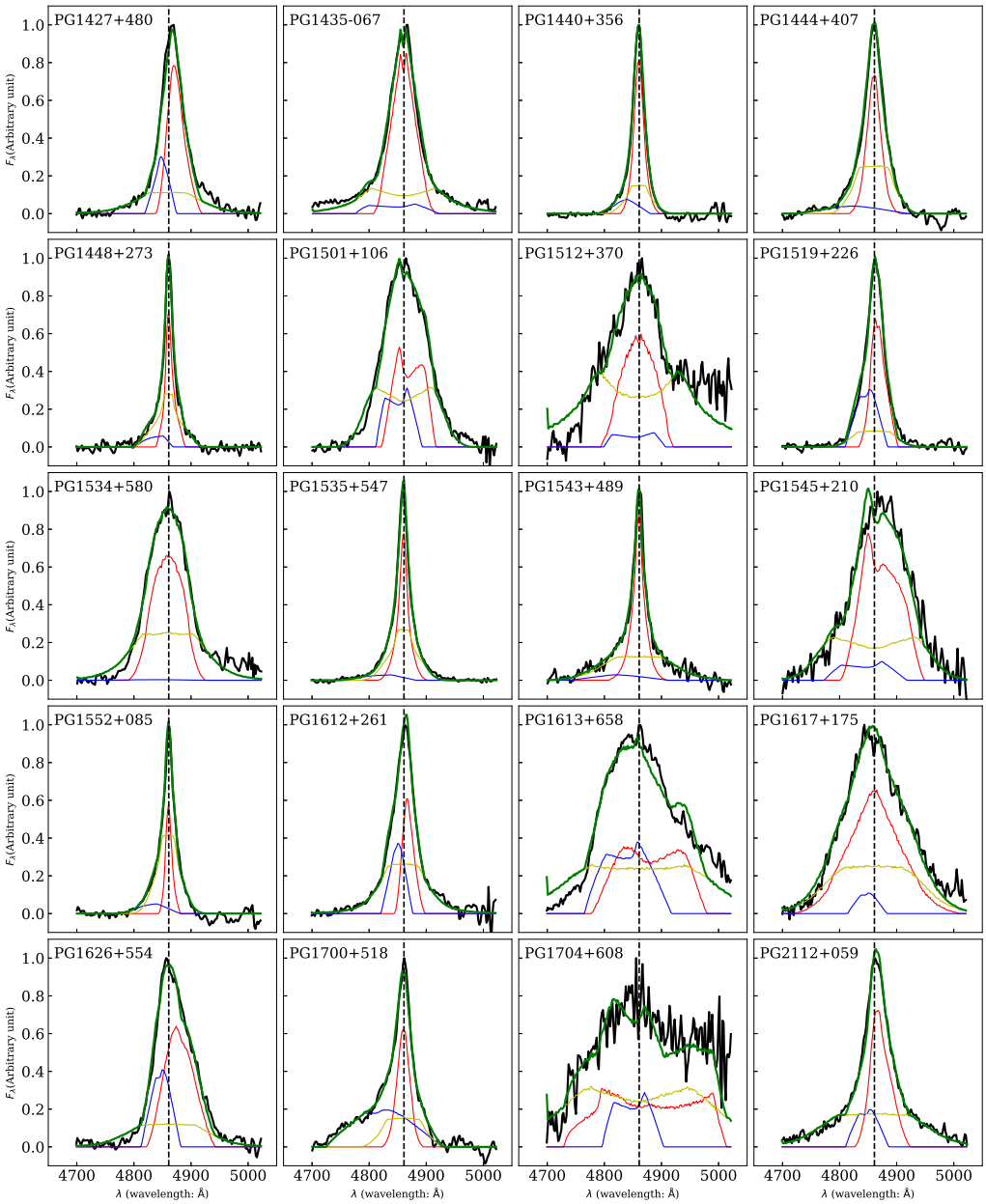

Supplementary Figure 1 *Continued*.

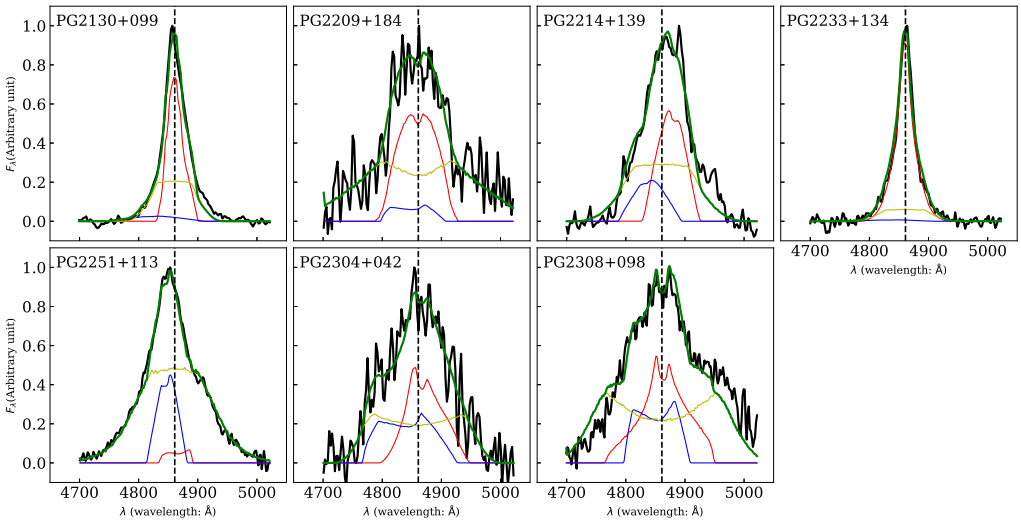

Supplementary Figure 1 *Continued*.

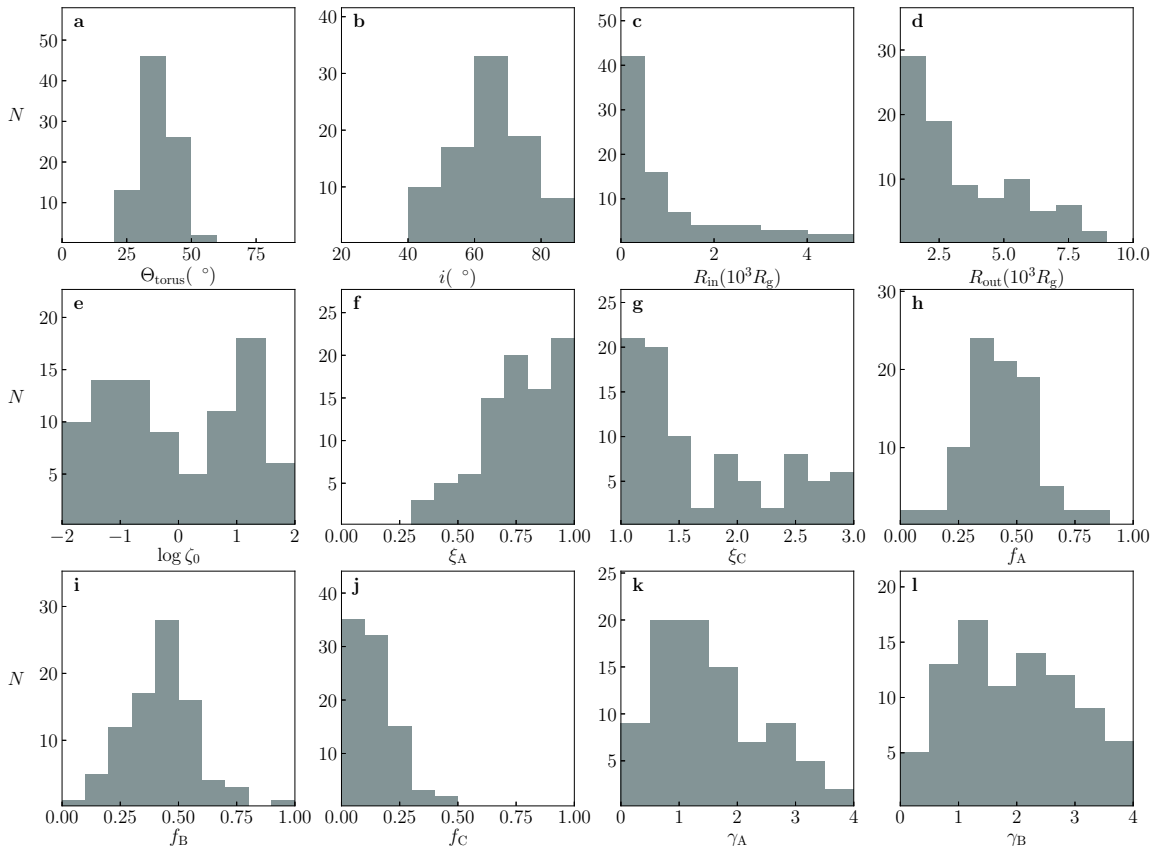

Supplementary Figure 2: **Distributions of the parameters obtained by fitting Hβ profiles.** Note $f_{\rm C} = 1-(f_{\rm A}+f_{\rm B})$, the average fraction of type C clouds is $\langle f_{\rm C}\rangle \approx 0.1$ and $f_{\rm C} \ll (f_{\rm B}, f_{\rm A})$ holds for most objects of the PG sample. There are a couple of objects with $\xi_{\rm C} \gtrsim 2$, potentially implying acceleration of type C clouds driven by radiation pressure, but this possibility needs to be explored by numerical simulations.

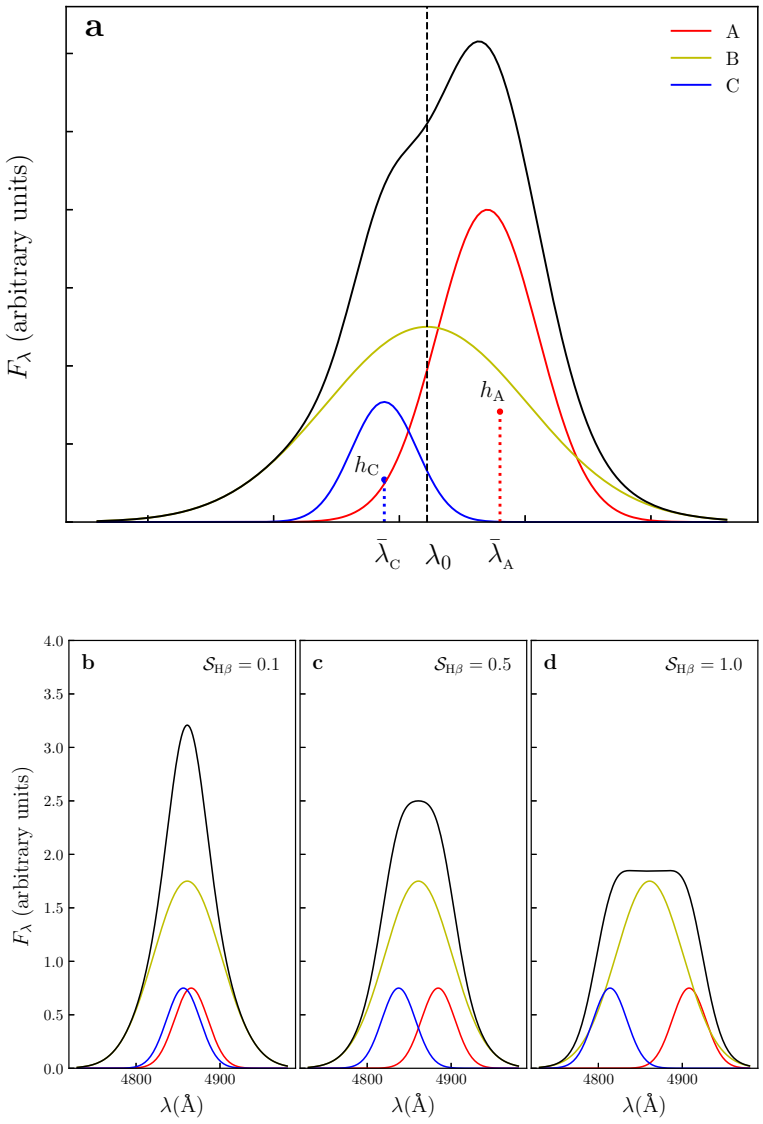

Supplementary Figure 3: **Illustration of physical meanings of parameters describing profiles.** Panel *a* shows a cartoon of decomposed profiles for physical meanings of the three parameters defined by Equation (16). The barycentre wavelength and fluxes are obtained by including flux-weight. As the first order approximation, the two parameters of $(h, \bar{\lambda})$ can completely describe individual profiles of the decomposed components and hence provide reasonable asymmetries, shapes and shifts of the total spectra. Panels *b-d* illustrate the relationship between $\mathcal{S}_{H\beta}$ and real shapes of profiles (from a triangular to boxy).

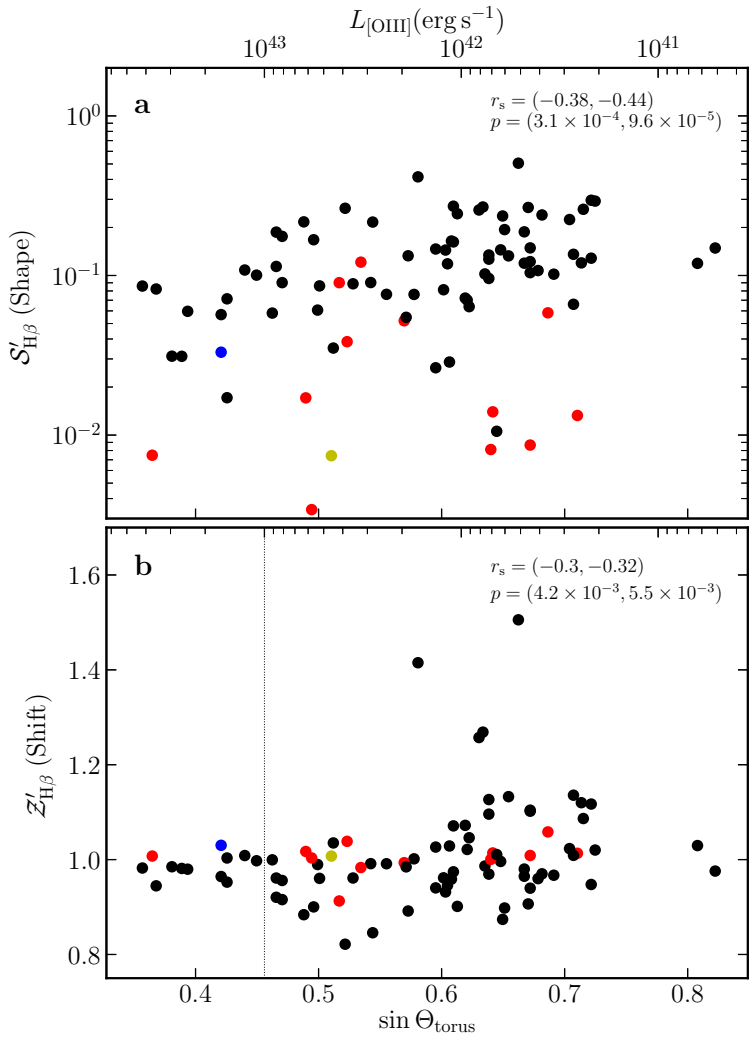

Supplementary Figure 4: **Correlations between $\mathcal{S}'_{\mathrm{H}\beta}$ and $\mathcal{Z}'_{\mathrm{H}\beta}$ versus $L_{[\mathrm{OIII}]}$.** Panel a shows a consistent correlation with panel *b* in Figure 4. There are four outliers with $\mathcal{Z}'_{\mathrm{H}\beta} \gtrsim 1.2$ deviating from the correlation in panel b. For objects with $L_{[\mathrm{OIII}]} \gtrsim 10^{43}\mathrm{erg\,s^{-1}}$, $\mathcal{Z}'_{\mathrm{H}\beta} \approx 1$ remains, which have smaller torus angles ($\Theta_{\mathrm{torus}} \lesssim 30°$).

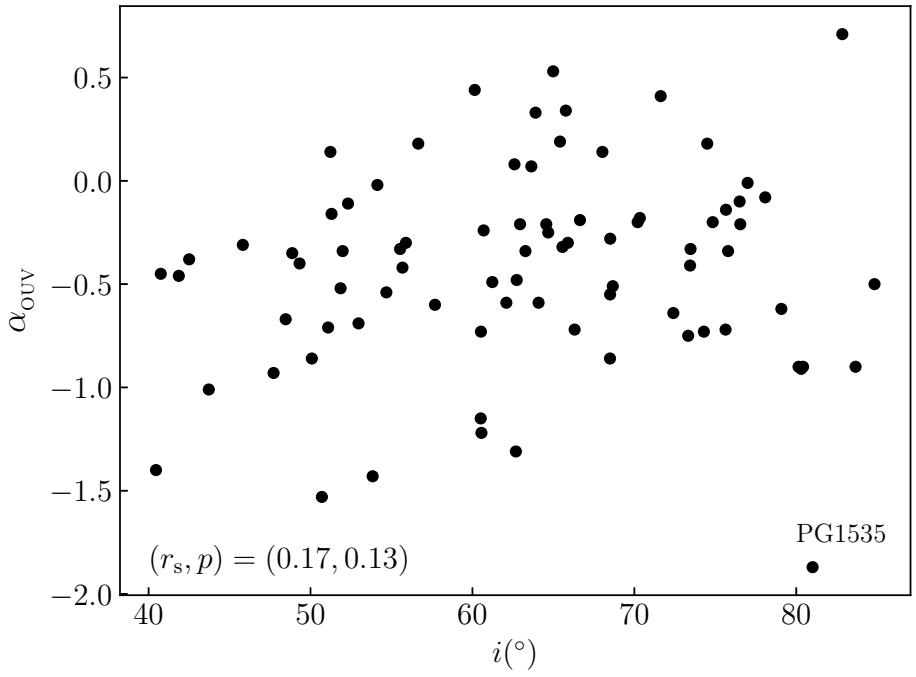

Supplementary Figure 5: **A comparison of PG quasar inclinations from the present model with $\alpha_{\rm OUV}$ as an orientation[2].** This shows that they are consistent with each others. The Spearman coefficient and null-probability are indicated in the plot except for PG 1535. Error bars of $\alpha_{\rm OUV}$ are not given by Ref.[2], and i is given in Supplementary Table 1.

1. Reyes, R. *et al.* Space density of optically selected type 2 quasars. *Astron. J.* **136,** 2373-2390 (2008).

2. Baskin, A. & Laor, A. What controls the C IV line profile in active galactic nuclei? *Mon. Not. R. Astron. Soc.* **356**, 1029−1044 (2005).